

Harmonic correlators for UHECRs

Federico R. Urban^{a,*}

^a*CEICO, FZU, Institute of Physics of the Czech Academy of Sciences,
Na Slovance 1999/2, 182 21 Prague, Czech Republic*

E-mail: federico.urban@fzu.cz

I will review the applications, advantages, limitations, and current status of harmonic techniques to detect anisotropies in the UHECR arrival direction distribution. In particular I will focus on the harmonic cross-correlation between the UHECR sky and galaxies, where the latter are taken as proxies for the locations of UHECR sources in the assumption that such sources correlate with the large-scale structure of the Universe. This type of harmonic cross-correlation has been proposed only recently, and it shows very promising complementarities with the well-known harmonic UHECR autocorrelation. After a brief introduction I will discuss novel tools and applications to account for different UHECR chemical composition and for the random deflections caused by the galactic magnetic field. I will show how the combination of UHECR harmonic auto-correlation and cross-correlations with large-scale structures can disentangle different UHECR primaries and could reverse-engineer some of the effects of the galactic magnetic field to a much better degree than the auto-correlation alone. I will conclude with an outlook on applications to other data sets, such as astrophysical neutrinos.

*37th International Cosmic Ray Conference (ICRC 2021)
July 12th – 23rd, 2021
Online – Berlin, Germany*

*Presenter

1. Introduction

The origin and chemical composition of charged ultra-high energy cosmic rays (UHECRs) are still a mystery since their discovery 60 years ago. We do not know what they are nor where they come from—or how they are pushed to such extreme energies [1].

From the nearly isotropic sky distribution of UHECRs we infer that the highest energy rays are extra-galactic, see, e.g., [2–4]. Extra-galactic sources are most probably correlated with the distribution of visible matter in the Universe, also known as the large-scale structure (LSS). The Universe is not transparent to UHECRs because it is filled with cold photons from the cosmic microwave background and the extragalactic background light. Therefore, UHECRs can propagate only for a few hundreds of Mpc, depending on their chemical composition. Within this volume the LSS is anisotropic, which implies that the UHECR flux distribution in the sky should bear the imprint of this anisotropy.

UHECRs do not propagate in a straight line from the source to the observer, but are instead deflected by intervening Galactic (GMF) and extra-Galactic magnetic fields. To further complicate this picture, UHECR chemical composition and magnetic field strength are degenerate when it comes to UHECRs deflections. Therefore, the relationship between the anisotropy of the LSS and that of UHECRs is non-trivial. Hunting for UHECR anisotropies requires striking a balance between the shot noise, which rapidly increases with energy as the number of detected events plummets, and the magnetic deflections that distort and suppress UHECR anisotropies, which instead decrease with energy.

The global features of an anisotropic flux distribution in the sky can be captured by the angular auto-correlation (AC), which, in harmonic space, takes the form of the angular power spectrum coefficients S_ℓ^{AC} . With current data the AC is dominated by the shot noise, making the underlying correlation with the LSS hard to detect [5, 6], although in some injection models low-multipoles could be within reach [7, 8].

A complementary harmonic observable is the harmonic-space cross-correlation (XC) between UHECR arrival directions and the distribution of galaxies on the sphere, first proposed in [9]. The logic is as follows: the flux of UHECRs in a given direction $\hat{\mathbf{n}} := (\vartheta, \varphi)$ can be decomposed in spherical harmonic coefficients as $\Phi^{\text{CR}}(\hat{\mathbf{n}}) = \sum_{\ell m} a_{\ell m}^{\text{CR}} Y_{\ell m}(\hat{\mathbf{n}})$. The same is true of the galaxy overdensity field: $\Phi^{\text{gal}}(\hat{\mathbf{n}}) = \sum_{\ell m} a_{\ell m}^{\text{gal}} Y_{\ell m}(\hat{\mathbf{n}})$. If both UHECRs and galaxies are tracing the same underlying distribution, namely the LSS, we expect that $a_{\ell m}^{\text{CR}} \propto a_{\ell m}^{\text{gal}}$. The harmonic AC and XC signal spectra are respectively given by

$$S_\ell^{\text{AC}} := \frac{1}{2\ell + 1} \sum_m a_{\ell m}^{\text{CR},*} a_{\ell m}^{\text{CR}}, \quad S_\ell^{\text{XC}} := \frac{1}{2\ell + 1} \sum_m a_{\ell m}^{\text{CR},*} a_{\ell m}^{\text{gal}}. \quad (1)$$

The XC stands apart from other observables for (at least) four reasons. First, systematic uncertainties of different fields, in this case UHECRs and galaxies, do not cross-correlate, and, under some conditions, statistical noises do not strongly cross-correlate either; this makes the XC an experimentally cleaner observable than the AC. Second, in the limit where the sources of UHECRs are numerous but the detected events are not, it is possible to take advantage of the much denser source sampling of the LSS to dramatically boost the signal-to-noise ratio (SNR) and the chances of detection with the XC. Third, the XC encode more astrophysical information

than the AC, because two fields typically respond differently to astrophysical parameters. Fourth, harmonic power spectra (in this case both the AC and the XC) have considerable mathematical and computational advantages over real-space correlators, because of their elegant and powerful mathematical description, and allow for a straightforward visualisation of the main components of the astrophysical model.

In this proceedings contribution we present theoretical results for three injection models: (a) a pure proton model (H1) with a power-law spectrum $\Phi^{\text{CR}} \propto E^{-\gamma}$ with slope $\gamma = 2.6$ at all energies; (b) a pure oxygen-16 model (O16) with spectral index $\gamma = 2.1$ at all energies; (c) a pure silicon-28 injection (Si28) with power $\gamma = 1.5$ and a sharp injection cutoff at $E = 280$ EeV. These models are the same as in [8] and are representative of the UHECR energy spectrum and composition fits with current experimental data. We study the propagation of the three injection models by following 10^6 events with *SimProp* v2r4 [10] with energies above $E = 10$ EeV for redshifts up to $z = 0.3$. In following the different nuclei, we adopt the same simplifications as in [8].

For each model we choose three energy cuts for the integral spectrum of UHECRs: $E_{\text{cut}} = 10^{19.6}$ eV $\simeq 40$ EeV, $E_{\text{cut}} = 10^{19.8}$ eV $\simeq 63$ EeV, and $E_{\text{cut}} = 10^{20}$ eV = 100 EeV. As a representative choice of what could be expected with current experimental facilities we use $N_{\text{CR}} = 1000$, $N_{\text{CR}} = 200$, and $N_{\text{CR}} = 30$ UHECR events over the full sky, for the three energy cuts defined above, respectively.

The last ingredient for the UHECR flux is the GMF—we ignore the, most probably subdominant and still hypothetical, extra-Galactic fields [11]. Our prescription for the GMF is to smear the map of UHECRs below a certain angular scale, which in our language is as simple as introducing a (Gaussian) beam in the signals as

$$\mathcal{S}_\ell^{\text{AC}} \rightarrow \mathcal{S}_\ell^{\text{AC}} \mathcal{B}_\ell^2, \quad \mathcal{S}_\ell^{\text{XC}} \rightarrow \mathcal{S}_\ell^{\text{XC}} \mathcal{B}_\ell, \quad (2)$$

where $\mathcal{B}_\ell := \exp[-\ell(\ell+1)\theta_{\text{smear}}^2/2]$ and θ_{smear} is the smearing angle. Even though the effects due to the GMF are not isotropic [12], we conservatively simplify the model by smearing uniformly with the maximal deflection angle given by $\theta_{\text{smear}} \approx 4.7 \left(\frac{40 \text{ EeV}}{E/Z}\right)$ deg where Z is the atomic number and E is the UHECR energy. We do not account for the large-scale galactic field, which can not be described by a simple smearing—its effects are going to be comparable but significantly more nuanced due to its coherent structure. We account for the energy dependence of the UHECR flux once it hits the GMF by binning the total flux in seven logarithmic energy bins with logarithmic width of 0.1, separately smearing each bin with an angle corresponding to the lowest energy in the bin, and adding them up proportionally to their share in the total number of events. Lastly, in the O16 model, where the composition on the edge of the Milky Way includes a significant fraction of protons mixed with heavier nuclei, we smear the two fluxes (protons and O16 nuclei) separately and then add up the signals.

The properties of the galaxy sample are modelled after the 2MASS Redshift Survey (2MRS) [13], which constitutes one of the most complete full-sky spectroscopic low-redshift surveys, generalised to the full sky.

Lastly, we apply a uniform Gaussian beam with FWHM of 1 deg to all spectra in order to take into account the approximately 1 deg angular resolution of current UHECR experiments.

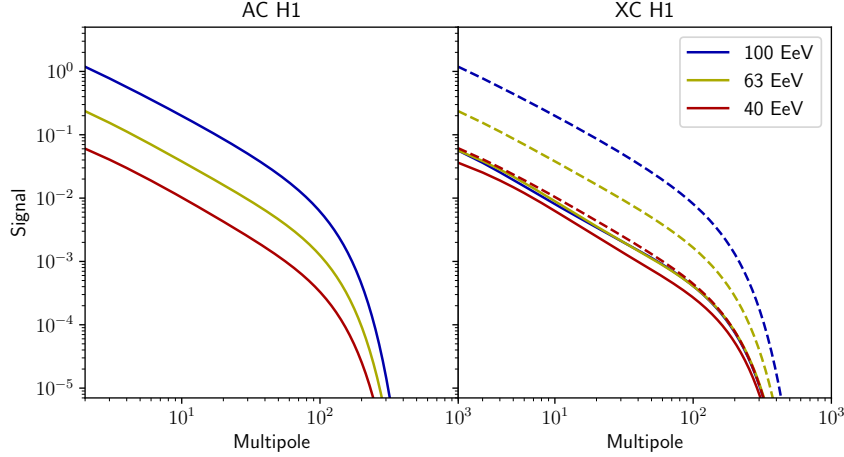


Figure 1: Signal power spectra for the H1 model, for the three energy cuts $E_{\text{cut}} = 40$ EeV (red lines), $E_{\text{cut}} = 63$ EeV (yellow lines) and $E_{\text{cut}} = 100$ EeV (blue lines). The left panel shows the AC, whereas the XC is on the right panel—dashed lines show the XC when optimal weights are employed.

2. Results

In Fig. 1 we show the signal power spectra for the H1 model. The XC is smaller than the AC, because the radial kernels, or the distribution of sources and events with distance, of the galaxy catalogue and the UHECR event set are different: the former peaks around redshift $z = 0.03$ whereas the latter monotonically decreases with redshift (there are fewer UHECRs from farther away). The dashed lines represent the XC when we employ *optimal weights*: these are weights that take into account the fact that farther sources will contribute fewer UHECRs at increasing energy, and can be computed once the UHECR attenuation function, as computed for instance from *SimProp*, is known. The fact that weighting galaxies according to UHECR energy losses is not only a physically sensible strategy but is in fact the optimal one for detection can be formally proven using our language, see the discussion in [9]—with optimal weights the AC and XC signal spectra are by definition the same. As expected, the power spectra tend to increase with increasing cutoff energy, because the distance travelled by UHECRs decreases and the anisotropies become more pronounced. The O16 and Si28 models (not shown) have larger signals because they are more strongly attenuated, hence, they travel shorter distances and bear a stronger anisotropic imprint.

In Fig. 2 we present the per- ℓ SNR for the AC (left) and XC (right) for the H1 model (no magnetic smearing). The XC power peaks at much higher multipoles, corresponding to smaller angular scales, than that of the AC. This means that the XC is most sensitive to anisotropies that are not detectable with the AC, and vice-versa. This highlights the complementarity of the two observables.

In Fig. 3 we turn our focus to the O16 model. As in the H1 case, the XC power peaks at much higher multipoles than that of the AC. For both AC and XC the best chances for detection are at low energy cuts because even if the signal is stronger for higher energies, the smaller number of events at high energies strongly suppresses the SNR.

Fig. 4 is for Si28, and illustrates once again that the XC power peaks at much higher multipoles

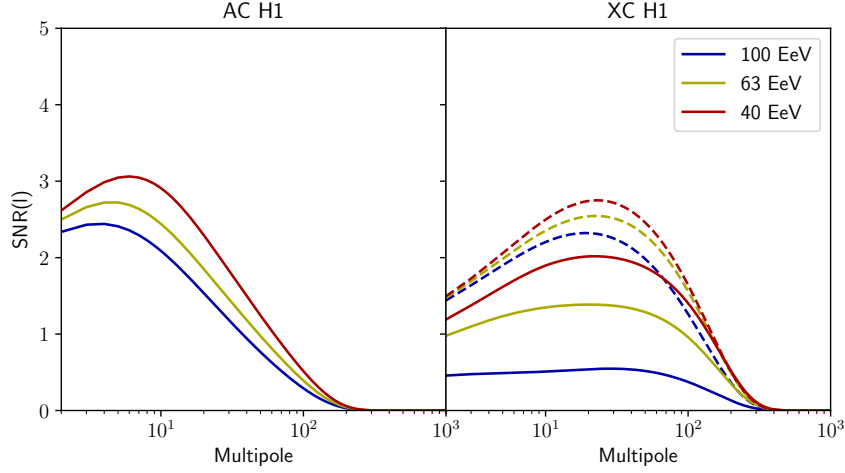


Figure 2: Per- l SNR for the AC (left panel) and XC (right panel) for the H1 model in absence of magnetic smearing; the same colour-coding as in Fig. 1 apply.

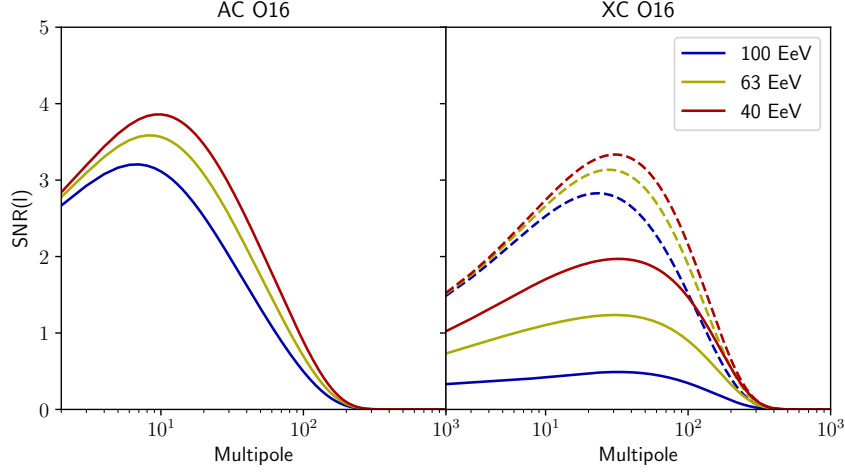


Figure 3: Per- l SNR for the AC (left panel) and XC (right panel) for the O16 model in absence of magnetic smearing; the same colour-coding as in Fig. 1 apply.

than that of the AC. Contrary to the H1 and O16 cases here the benefits of a shorter propagation length at higher energies outweigh the increase in shot noise due to the drop in number of events: the best chances for detection are at the highest energy cut we consider, 100 EeV, with 20 events only. This applies to both AC and XC, but in the latter case only if optimal weights are applied.

Fig. 5 (H1 model with magnetic smearing) shows how the power at high multipoles is suppressed by the magnetic deflections. Moreover, for the XC with optimal weights we observe how a higher energy cut improves the chances for detection: the smaller propagation distance combined with the smaller magnetic deflections win over the higher shot noise caused by the smaller number of UHECR events.

In Fig. 6 we see how the power for both the AC and XC is severely suppressed by the GMF in the O16 model. Nonetheless, the total SNRs are in the detectable range for both observables.

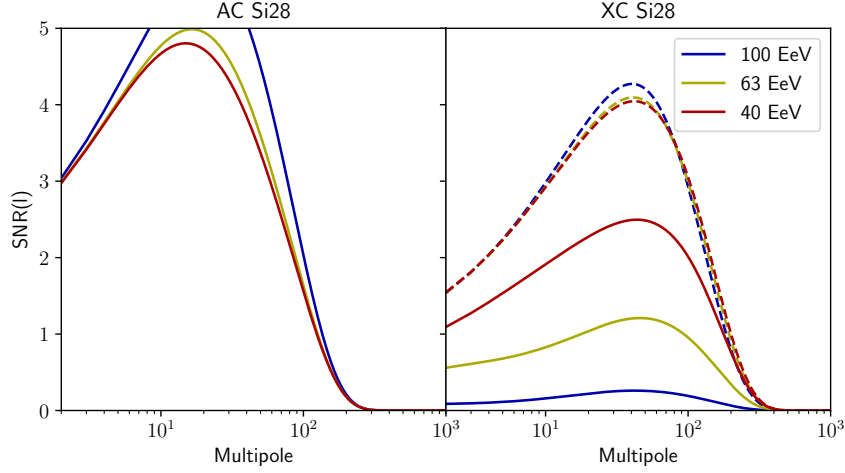


Figure 4: Per- ℓ SNR for the AC (left panel) and XC (right panel) for the Si28 model in absence of magnetic smearing; the same colour-coding as in Fig. 1 apply.

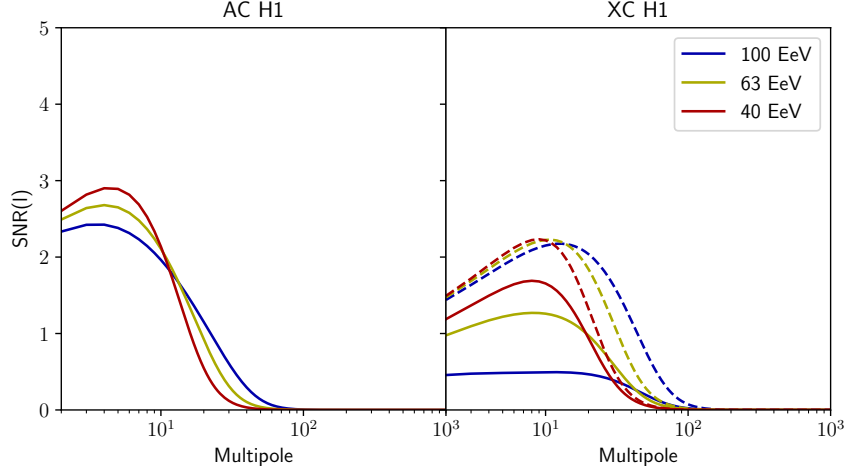


Figure 5: Per- ℓ SNR for the AC (left panel) and XC (right panel) for the H1 model with magnetic smearing; the same colour-coding as in Fig. 1 apply.

We also note, in the case of the XC at the highest energies, the “two bumps” structure due to the mixture of protons and heavy nuclei after propagation, with vastly different deflection angles.

Fig. 7 shows how the power for both the AC and XC is even more severely suppressed by the strong magnetic deflections than in the O16 case. The total SNRs are nearly detectable; with more events and with a more physical model for the deflections, one that accounts for the fact that the deflections decrease with galactic latitude, this signal could be detectable.

3. Conclusions and outlook

We have shown how the harmonic XC is a new tool complementary to the AC, and could be detected for a range of energies and injection models. In particular, the XC performs better than

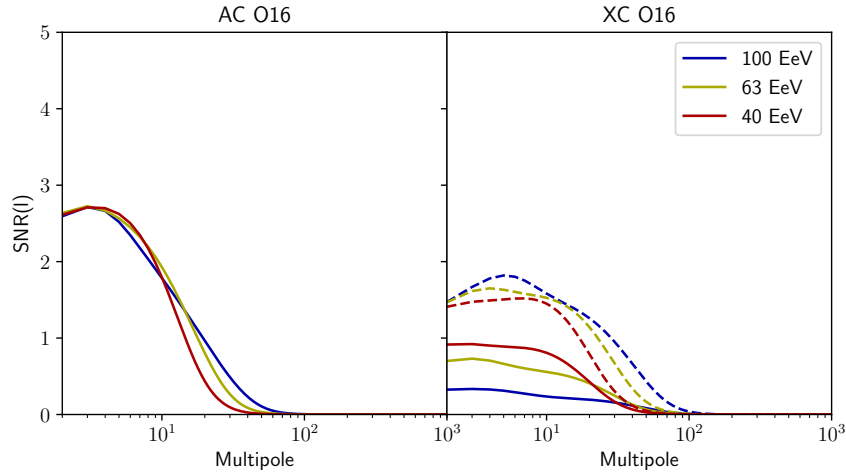


Figure 6: Per- ℓ SNR for the AC (left panel) and XC (right panel) for the O16 model with magnetic smearing; the same colour-coding as in Fig. 1 apply.

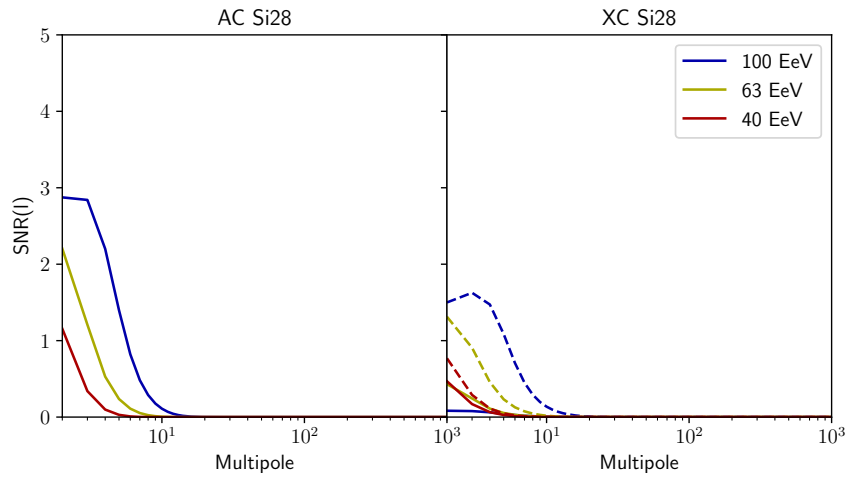


Figure 7: Per- ℓ SNR for the AC (left panel) and XC (right panel) for the Si28 model with magnetic smearing; the same colour-coding as in Fig. 1 apply.

the AC at high-multipoles. Matching the UHECR and galaxy catalogue kernels has a strong impact on the XC: therefore, it could be possible to use this effect to reverse-engineer the injection model (which defines the radial kernel). Moreover, the AC and XC are sensitive to the injection properties and magnetic deflections in different ways, which could make it possible to disentangle the two. The same harmonic techniques can be applied to other datasets that track the LSS, for example the thermal Sunyaev-Zeldovich intensity, which is very accurate down to angles much smaller than a degree, and peaks at zero redshift [14]. Likewise, this technique can prove valuable in the case of other messengers such as astrophysical neutrinos [15].

References

- [1] R. Alves Batista et al., *Open Questions in Cosmic-Ray Research at Ultrahigh Energies*, *Front. Astron. Space Sci.* **6** (2019) 23 [1903.06714].
- [2] P.G. Tinyakov, F.R. Urban, D. Ivanov, G.B. Thomson and A.H. Tirone, *A signature of EeV protons of Galactic origin*, *Mon. Not. Roy. Astron. Soc.* **460** (2016) 3479 [1511.01333].
- [3] R.U. Abbasi et al., *Search for EeV Protons of Galactic Origin*, *Astropart. Phys.* **86** (2017) 21 [1608.06306].
- [4] PIERRE AUGER collaboration, *Observation of a Large-scale Anisotropy in the Arrival Directions of Cosmic Rays above 8×10^{18} eV*, *Science* **357** (2017) 1266 [1709.07321].
- [5] PIERRE AUGER, TELESCOPE ARRAY collaboration, *Full-sky searches for anisotropies in UHECR arrival directions with the Pierre Auger Observatory and the Telescope Array*, *PoS ICRC2019* (2020) 439 [2001.01864].
- [6] O. Deligny, *Large-Scale Distribution of Arrival Directions of Cosmic Rays Detected at the Pierre Auger Observatory and the Telescope Array (ICRC2015)*, *PoS ICRC2015* (2015) 395.
- [7] P.G. Tinyakov and F.R. Urban, *Full sky harmonic analysis hints at large ultra-high energy cosmic ray deflections*, *J. Exp. Theor. Phys.* **120** (2015) 533 [1411.2486].
- [8] A. di Matteo and P. Tinyakov, *How isotropic can the UHECR flux be?*, *Mon. Not. Roy. Astron. Soc.* **476** (2018) 715 [1706.02534].
- [9] F.R. Urban, S. Camera and D. Alonso, *Detecting ultra-high energy cosmic ray anisotropies through cross-correlations*, 2005.00244.
- [10] R. Aloisio, D. Boncioli, A. Di Matteo, A.F. Grillo, S. Petrerera and F. Salamida, *SimProp v2r4: Monte Carlo simulation code for UHECR propagation*, *JCAP* **1711** (2017) 009 [1705.03729].
- [11] M.S. Pshirkov, P.G. Tinyakov and F.R. Urban, *New limits on extragalactic magnetic fields from rotation measures*, *Phys. Rev. Lett.* **116** (2016) 191302 [1504.06546].
- [12] M.S. Pshirkov, P.G. Tinyakov and F.R. Urban, *Mapping UHECRs deflections through the turbulent galactic magnetic field with the latest RM data*, *Mon. Not. Roy. Astron. Soc.* **436** (2013) 2326 [1304.3217].
- [13] J.P. Huchra et al., *The 2MASS Redshift Survey - Description and Data Release*, *Astrophys. J. Suppl.* **199** (2012) 26 [1108.0669].
- [14] J. Erler, K. Basu, J. Chluba and F. Bertoldi, *Planck's view on the spectrum of the Sunyaev-Zeldovich effect*, *Mon. Not. Roy. Astron. Soc.* **476** (2018) 3360 [1709.01187].
- [15] K. Fang, A. Banerjee, E. Charles and Y. Omori, *A Cross-Correlation Study of High-energy Neutrinos and Tracers of Large-Scale Structure*, 2002.06234.